Towards the assimilation of radar reflectivities: Considering beam blockage in the observation operator

Günther Haase* and Eric Wattrelot

March 15, 2010

1 Introduction

Currently, Météo-France is developing a numerical weather prediction (NWP) model for the convective scale. This system, called AROME (Application de la Recherche à l'Opérationel à Méso-Echelle), covers France with 2.5 km horizontal resolution. It uses a three-dimensional variational (3DVar) data assimilation scheme and has an advanced representation of the water cycle with five hydrometeor classes (cloud water, rainwater, primary ice, snow and graupel) governed by a bulk microphysics parameterization.

The assimilation of radar reflectivities, thoroughly described in Wattrelot et al. (2008) and Montmerle et al. (2008), basically consists of three steps:

- simulate reflectivities from the model hydrometeors using an observation operator (Caumont et al., 2006),
- retrieve columns of pseudo-observations of humidity and other model prognostic variables from a reflectivity column, and
- assimilate the pseudo-observations through the 3DVar assimilation scheme.

*SMHI, S-60176 Norrköping (gunther.haase@smhi.se).

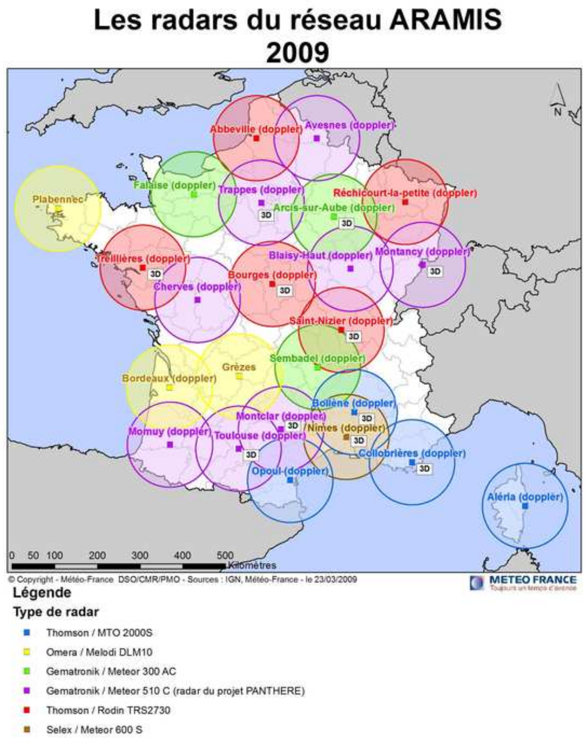

Figure 2.1: French radar network. The radius of the circles is 100 km and the color code corresponds to the different radar types.

2 Radar data

The French radar network (also called ARAMIS) consists of 24 radars (Figure 2.1), most of them are equipped with Doppler technology and some can measure dual polarization. A detailed description of the operational single radar and composite QPE products at Météo-France is given by Parent du Châtelet et al. (2006).

Data assimilation applies reflectivities from each individual radar within the operational measurement radius of 250 km. In a first step, polar volume data is averaged to a conical cartesian grid of 1×1 km^2. Pixels from different elevation scans are assigned to the same geo-location as the corresponding pixel in the lowest elevation scan. Advection is applied in order to synchronize the different elevation scans carried out within 15 minutes.

The distance to the radar is used as quality measure through the observation error covariances: the larger the distance the lower is the weight of the observation in comparison to the model background. Radar data is stored in BUFR format and contain additionally a quality flag allowing to distinguish precipitation from spurious echoes (e.g. ground clutter).

In this study we focus mainly on the radars in Momuy, Toulouse, Opoul and Bollène as they are

Table 1: Radar sites in Southern France.

	Momuy	Toulouse	Opoul	Bollène
Latitude [°N]	43.62	43.57	42.92	44.32
Longitude [°E]	-0.61	1.38	2.86	4.76
Antenna height a.s.l. [m]	146	187	717	325
Lowest elevation angle [deg]	0.4	0.8	0.6	0.4
Half-power beam width [deg]	1.1	1.1	1.3	1.3

heavily affected by beam blockage. The characteristics of these radars are sumarized in Table 1.

3 Concept

It is well-known that beam blockage affects radar observations in complex terrain (see e.g. Germann and Joss, 2003). The screening effect of topography is likely to occur at low elevation angles, the most useful for radar precipitation estimation and also for reflectivity assimilation. Depending on the atmospheric conditions beam blockage can vary considerably.

3.1 Beam propagation model

At the Norwegian Meteorological Institute (met.no) Gjertsen and Dahl (2002) developed a beam propagation model (BPM) to correct errors in CAPPI products related to topographical beam blockage. They simulate the radar's field of view using information on the scan geometry, the vertical profile of refractivity, and a digital elevation model (DEM). The beam paths are computed by a geometrical-optics approach taking into account the atmospheric conditions. It is assumed that the local refractivity profile at the radar site is representative for the entire radar volume. Standard output fields of the BPM are e.g. the degree of beam blockage and the corresponding correction factor which can be applied to operational radar products (Bech et al., 2007).

If no refractivity profiles is specified beam propagation is simulated according to a vertical refractivity gradient corresponding to the US standard atmosphere. To simulate anomalous propagation it is possible to use atmospheric profiles from radiosondes or NWP model forecasts which are representative for the radar site. Note that operational NWP models can provide information with high temporal and spatial resolution but they still suffer from an inadequate description of the atmospheric boundary layer.

3.2 Visibility

There are a couple of options how to handle radar beam blockage in data assimilation. A pragmatic approach is to blacklist data which are potentially affected by clutter or beam blockage. In practice the lowest elevation scan(s) would be excluded from data assimilation to avoid the detrimental impact of contaminated data. In doing so even clean pixels might be rejected unnecessarily. Additionally, removing large amounts of data might cause problems when spreading positive increments of specific humidity in the model, i.e. it is not beneficial to not have any pixel assimilated in some areas. Another possibility is to employ maps of partial masks (e.g. produced from long-term averaged reflectivity maps and the Surfilum Software (Delrieu et al., 1995) which uses a high-resolution DEM) making it possible to balance the impact of data in the assimilation. Finally, the observed reflectivities could be corrected for topographical beam blockage. However, this might be difficult for strong rates of shielding. Instead we propose to consider beam blockage directly in the observation operator for radar reflectivities.

Thereunto we adopted the concept of visibility. Hereafter visibility is defined as the minimum height above sea level detectable by the radar main lobe. It depends obviously on the topography and the type of beam propagation, but also on the lowest elevation angle of the radar.

In this study we employed AROME's topography interpolated onto the radar grid (Figures A.1(a), A.2(a), A.3(a) and A.4(a)). As each grid point represents the mean value over an area of 1×1 km^2, model and real topography can differ considerably in complex terrain. Sometimes, the radar antenna height is several hundreds of meters above the model topography.

Figures A.1(b), A.2(b), A.3(b) and A.4(b) show the degree of beam blockage for the lowest elevation angle simulated with the BPM for the Momuy, Toulouse, Opoul and Bollène radar, respectively. To derive visibility maps from the BPM the radar volume is sampled with 0.1° resolution starting a half beam width below the lowest elevation angle. In other words, the beam center of the visibility simulation is defined by

$$\Phi_{vis} = \Phi_{low} - 0.5\Delta\Phi_{low} + 0.5\Delta\Phi_{vis} \ , \tag{3.1}$$

where Φ_{low} and $\Delta\Phi_{low}$ are the elevation angle and the beam width of the lowest elevation scan, respectiviely. The beam width of the visibility scan ($\Delta\Phi_{vis}$) should be large enough to overshoot the topography. In this study $\Delta\Phi_{vis}$ is set to 50° to cover also higher elevation angles. The beam center of the visibility scan is constant during the simulation and independent of topography. Figures A.1(c), A.2(c), A.3(c) and A.4(c) show the visibility maps applying the BPM configuration mentioned above. The corresponding elevation angles (Figures A.1(d), A.2(d), A.3(d) and A.4(d)) are computed according to

$$\phi_{vis} = \arcsin\left(\frac{(h_{vis} + R_e - h_{rad})^2 - r^2 - R_e^2}{2rR_e}\right) \ , \tag{3.2}$$

where h_{vis} is the minimum detectable height (i.e. visibility), h_{rad} is the height of the radar antenna, r is the range from the radar to the point of interest, $R_e = 4/3R$, and R is the earth's radius. Note that all BPM simulations are performed assuming standard propagation conditions.

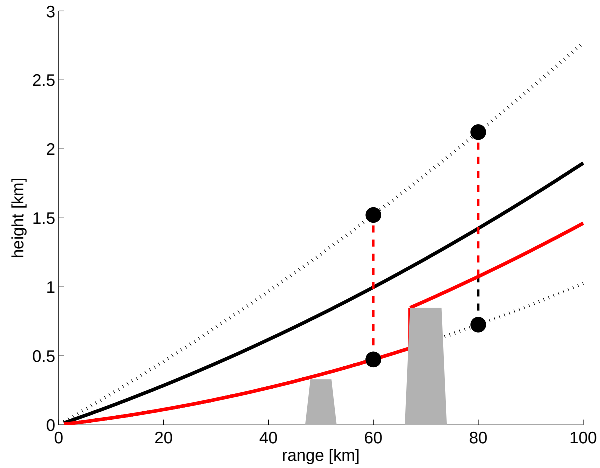

Figure 3.1: Vertical interpolation from model to radar space along the dashed lines (circles indicate the integration limits). The black solid line corresponds to the beam center (Φ_{low}) while the dotted lines mark the beam width ($\Delta\Phi_{low}$) of the unblocked beam. The red solid line defines the visibility (h_{vis}) assuming atmospheric standard conditions. Simulated reflectivities below the minimum detectable height are ignored.

3.3 Observation operator

The interpolation of variables from model space (model levels) to radar space (beam center) is part of the observation operator for reflectivities. Figure 3.1 illustrates the vertical interpolation with and without beam blockage assuming a Gaussian-shaped beam. Currently, topographical beam blockage is not considered in the radar observation operator. This might cause problems in mountainous regions where the interpolation considers model levels which are not visible by the radar (Figure 3.1 at 80 km). By using BPM's visibility maps for standard propagation the vertical interpolation becomes more realistic where the radar beam is completely or partly blocked. In this case the simulated reflectivities below the minimum detectable height (i.e. visibility) are ignored while the Gaussian weighting remains untouched.

4 Case study

The AROME model (cycle 35t2) was run over 48 hours for a case study initialised on 21 October 2009 1800 UTC. Three experiments with an rapid update cycle (RUC) of 3 hours have been carried out:

- control run with blacklisted radar reflectivity scans (759X)
- control run without blacklisted radar reflectivity scans (759Y)

- model run including visibility maps for all French radars but without blacklisted radar reflectivity scans (759Z)

Figures B.1 and B.2 show the reflectivity composites for the period 21 October 2009 1200 UTC till 23 October 2009 1200 UTC. Note that for 0000 UTC no radar composites exist.

Figure 4.1 gives an overview about the status of the data used for assimilation. The number of active data is considerably higher in the visibility run (759Z) compared to the reference experiment (759X), i.e. more data are used for assimilation. On the other hand, the number of rejected data is quite similar for both runs. The blacklisted data in 759Y and 759Z are Doppler winds.

Figure 4.2 shows the RMS and the bias for experiment 759Z versus reference experiments 759X and 759Y regarding radiosonde observations in the northern hemisphere. There are no significant differences in the meridional wind and the temperature bias. Focussing on the lower troposphere, the zonal wind bias for 759Z is slightly larger than in both reference experiments, however, the humidity bias is much less which gives hope that the new method improves the humidity distribution.

Figure 4.3 shows the accumulated precipitation according to experiment 759X, experiment 759Z, and rain gauges. At day one (21 October 2009) the two model runs hardly differ. However, at day two (22 October 2009) there is a slight improvement visible for the 759Z experiment at least for the highest precipitation threshold.

5 Future plans

Some ideas for further improvement of the proposed method:

- a more realistic topography would improve the quality of the visibility maps
- alternatively, the topography gradient around the radar station could be used to estimate the antenna height error
- consider anomalous beam propagation (AP) in the visibility simulation using e.g. the atmospheric fields from AROME.

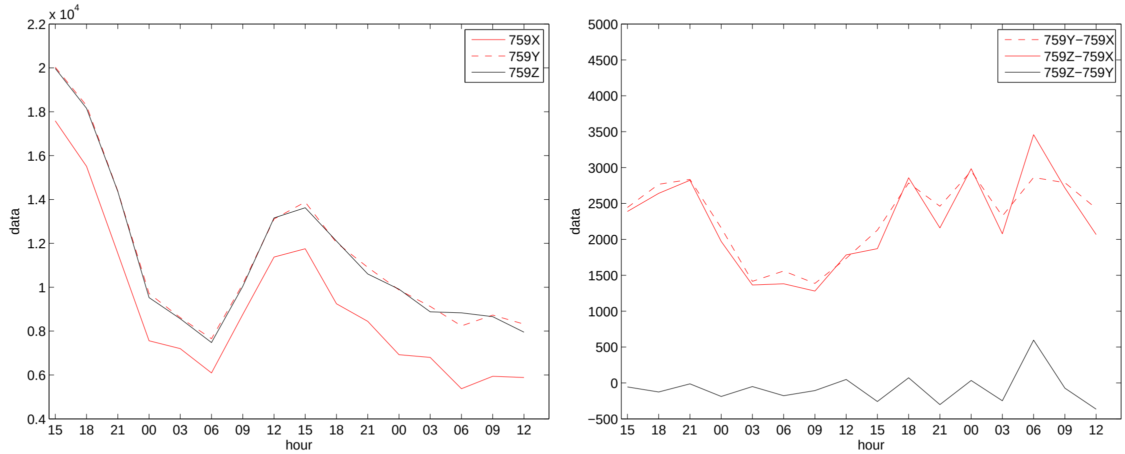

(a) Active data

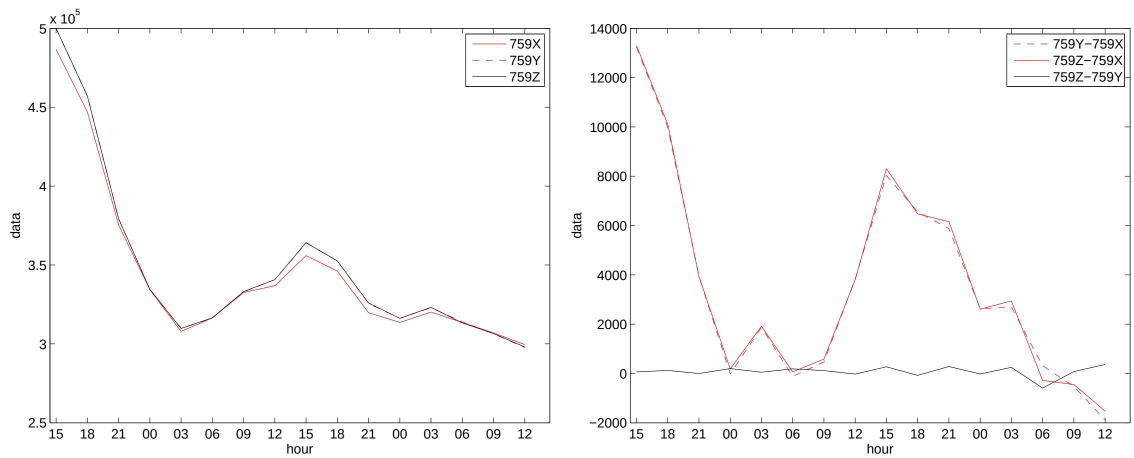

(b) Rejected data

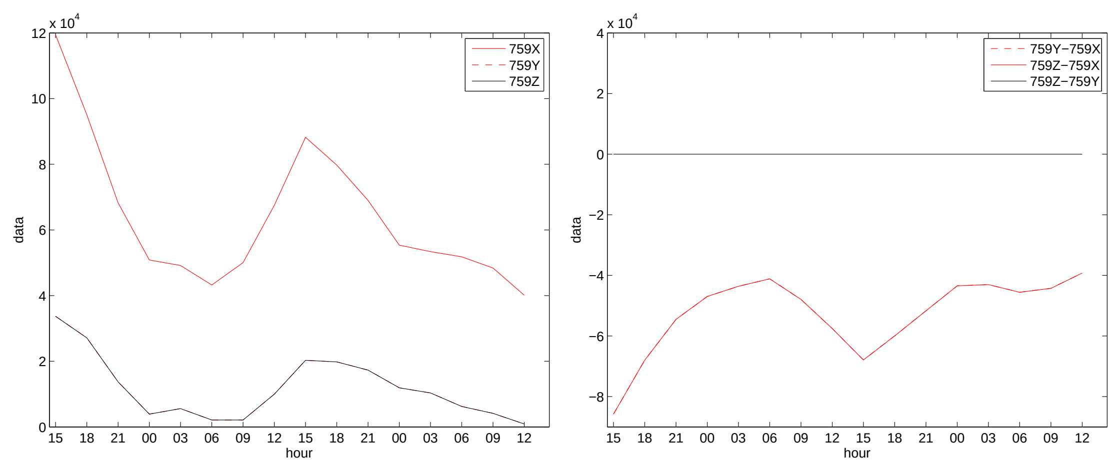

(c) Blacklisted data

Figure 4.1: Status of the data used for assimilation. The time axis starts at 21 October 2009 1500 and ends at 23 October 2009 1200.

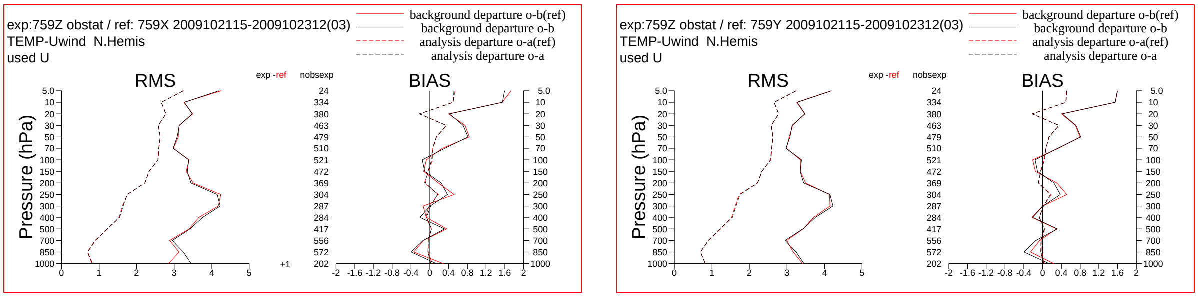

(a) TEMP u-wind

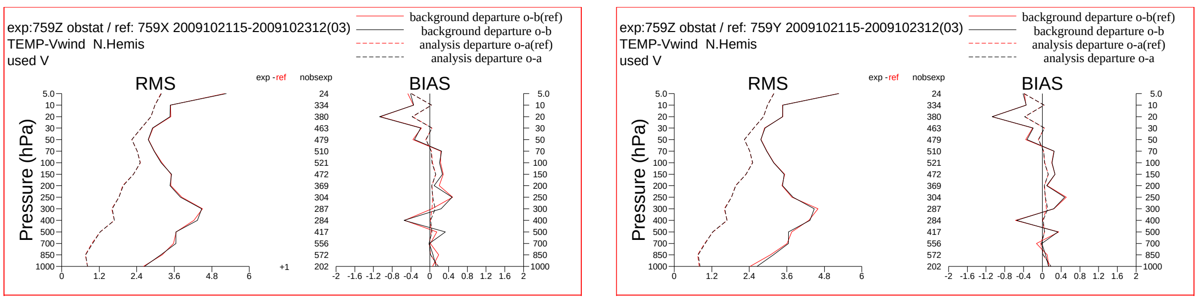

(b) TEMP v-wind

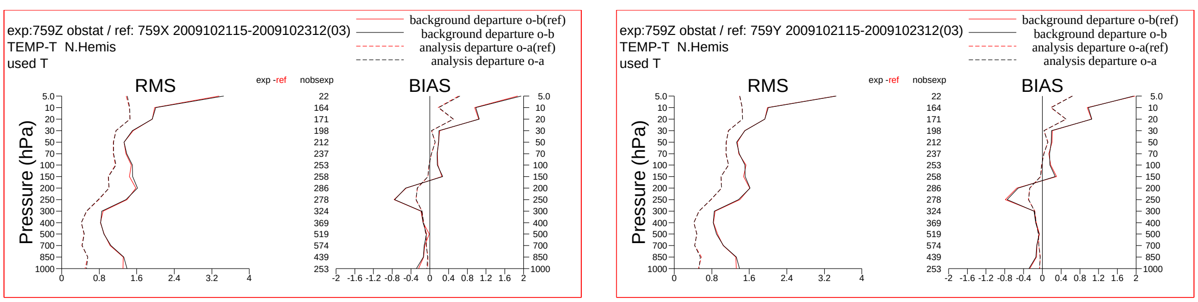

(c) TEMP temperature

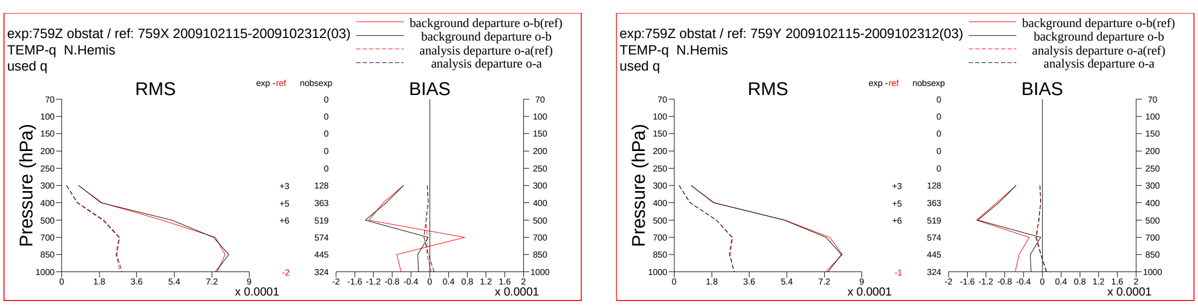

(d) TEMP humidity

Figure 4.2: RMS and bias for experiment 759Z versus reference experiments 759X (left) and 759Y (right).

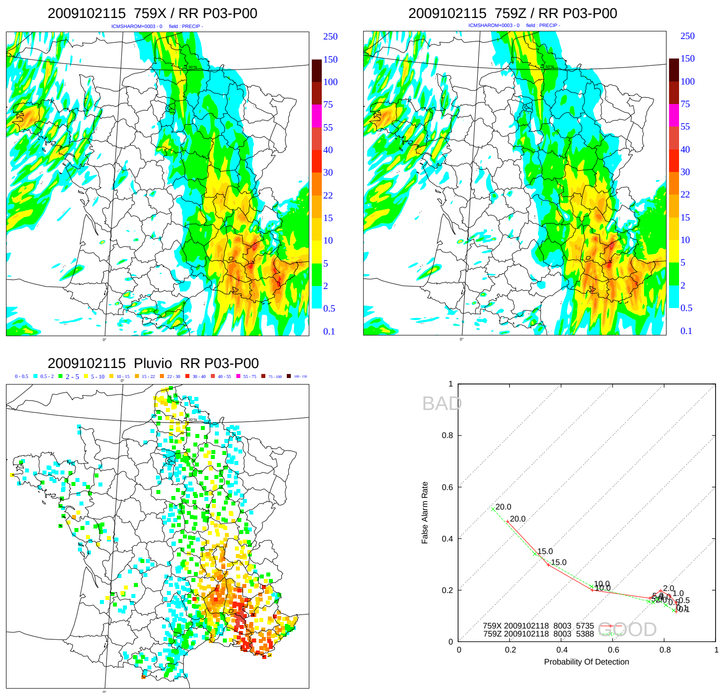

(a) 21 October 2009 1200-1500 UTC

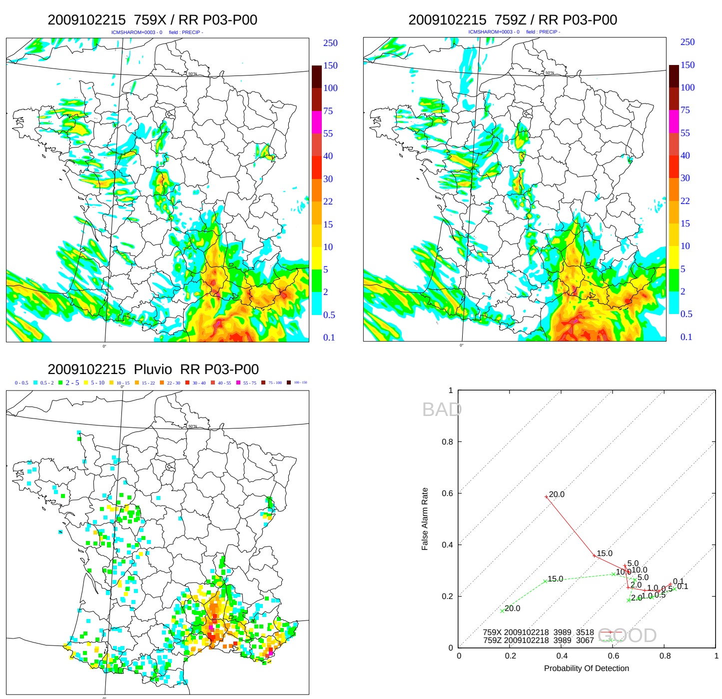

(b) 22 October 2009 1200-1500 UTC

Figure 4.3: Accumulated precipitation according to experiment 759X (upper left), experiment 759Z (upper right), and rain gauges (lower left). The corresponding skill scores for different precipitation thresholds are also shown (lower right).

A BPM simulations

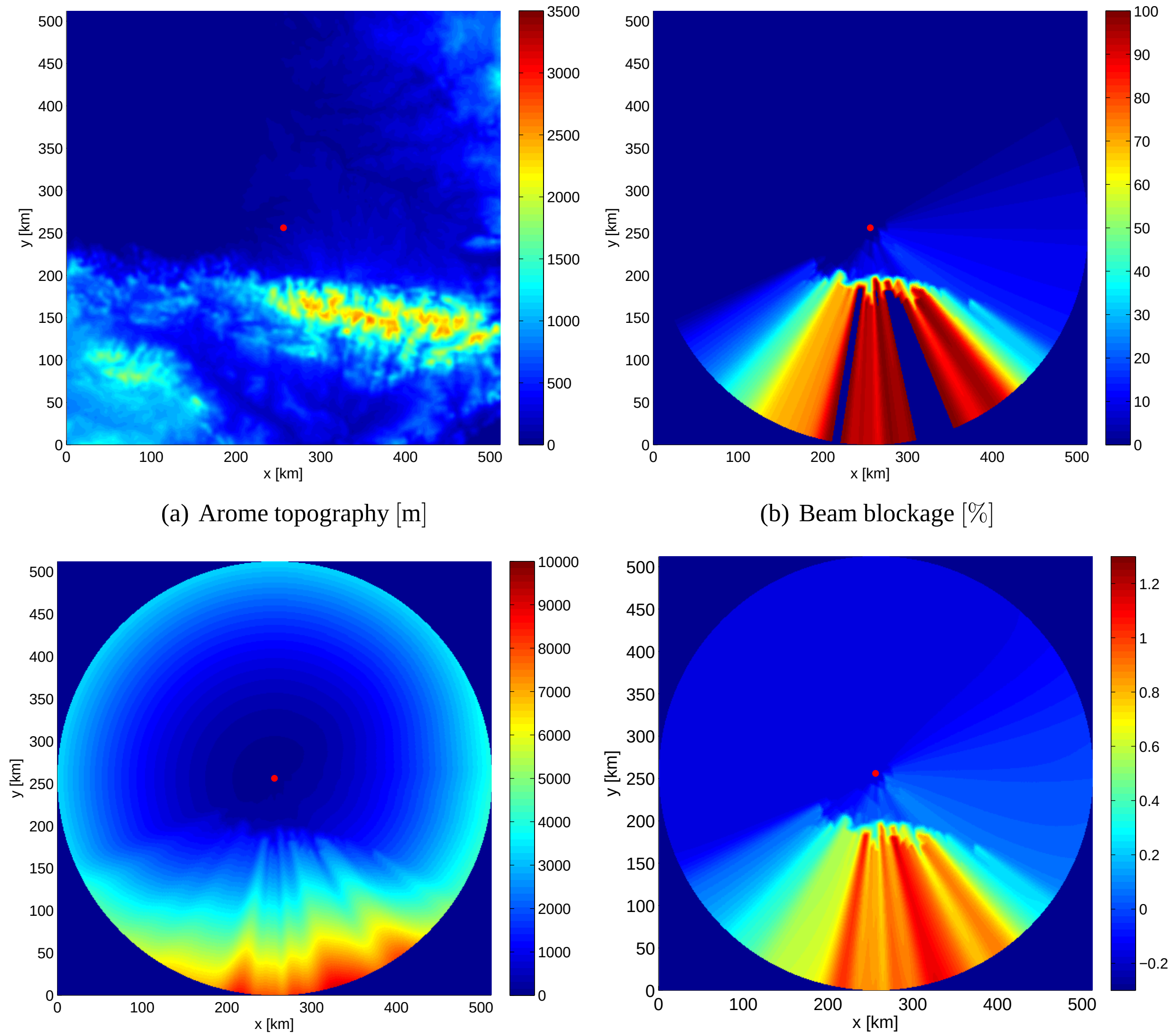

(a) Arome topography [m]

(b) Beam blockage [%]

(c) Visibility [m]

(d) Elevation angle corresponding to visibility [deg]

Figure A.1: BPM simulations for Momuy radar assuming standard propagation.

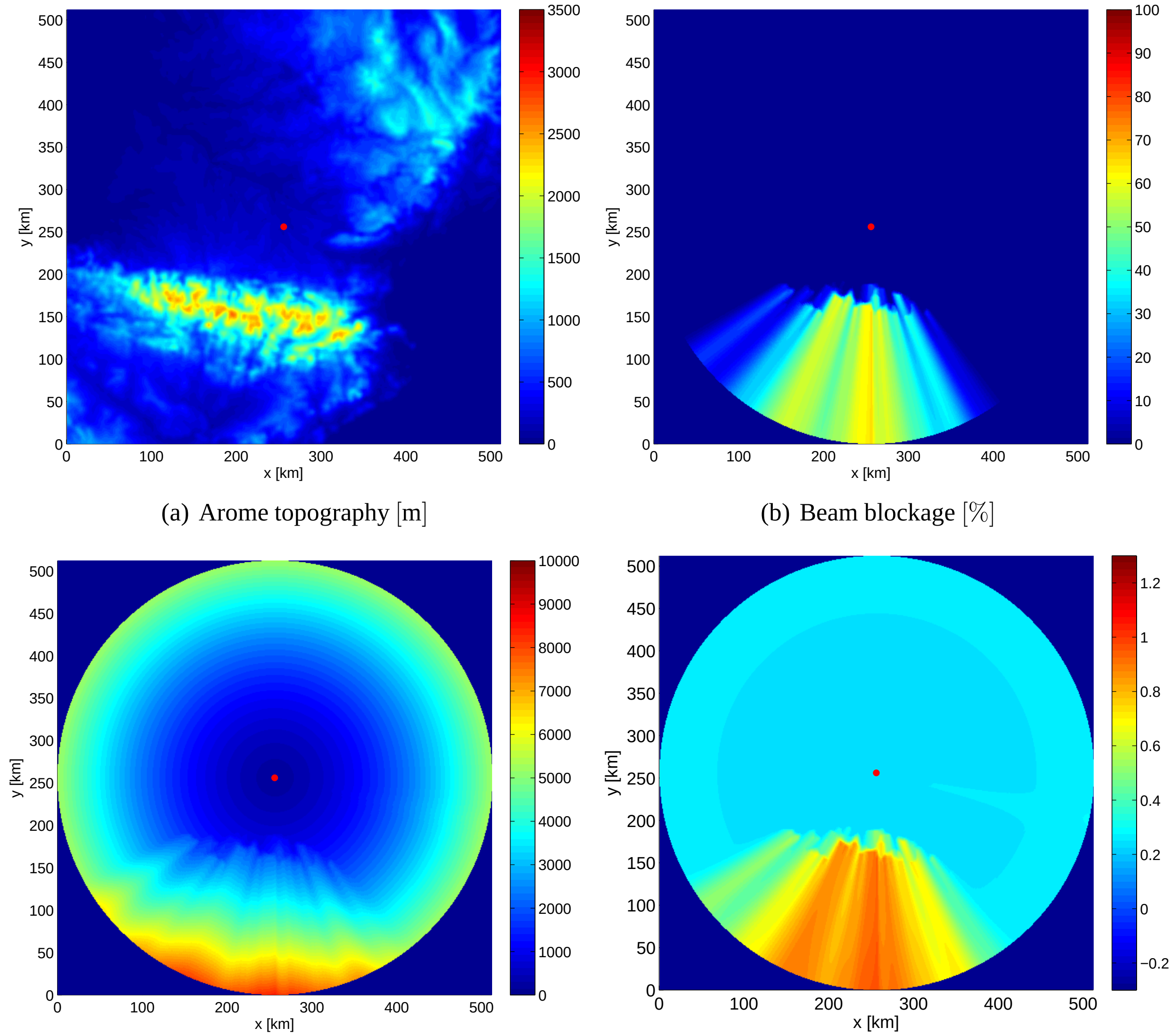

(a) Arome topography [m]

(b) Beam blockage [%]

(c) Visibility [m]

(d) Elevation angle corresponding to visibility [deg]

Figure A.2: BPM simulations for Toulouse radar assuming standard propagation.

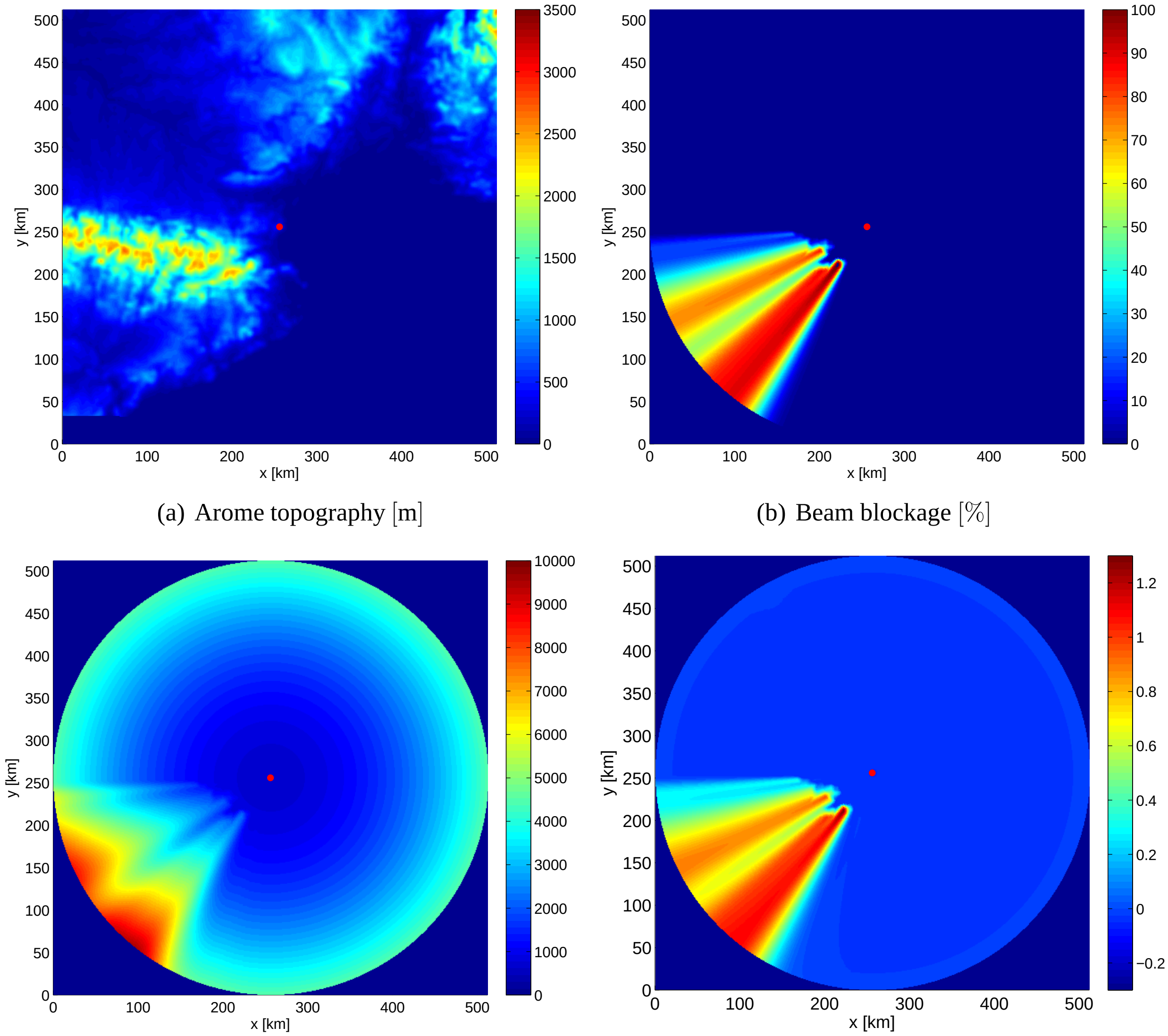

(a) Arome topography [m]

(b) Beam blockage [%]

(c) Visibility [m]

(d) Elevation angle corresponding to visibility [deg]

Figure A.3: BPM simulations for Opoul radar assuming standard propagation.

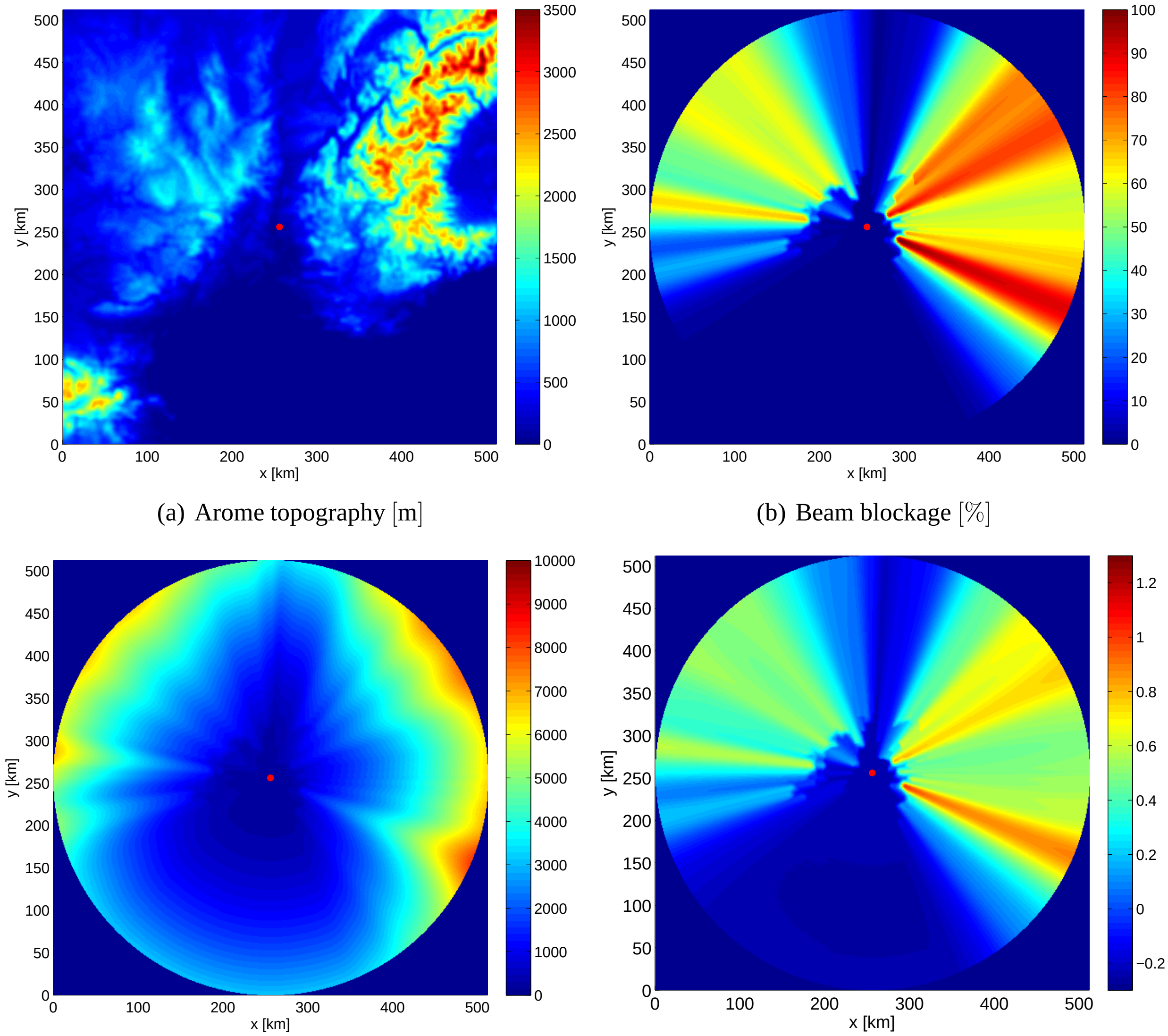

(a) Arome topography [m]

(b) Beam blockage [%]

(c) Visibility [m]

(d) Elevation angle corresponding to visibility [deg]

Figure A.4: BPM simulations for Bollène radar assuming standard propagation.

B Radar imagery

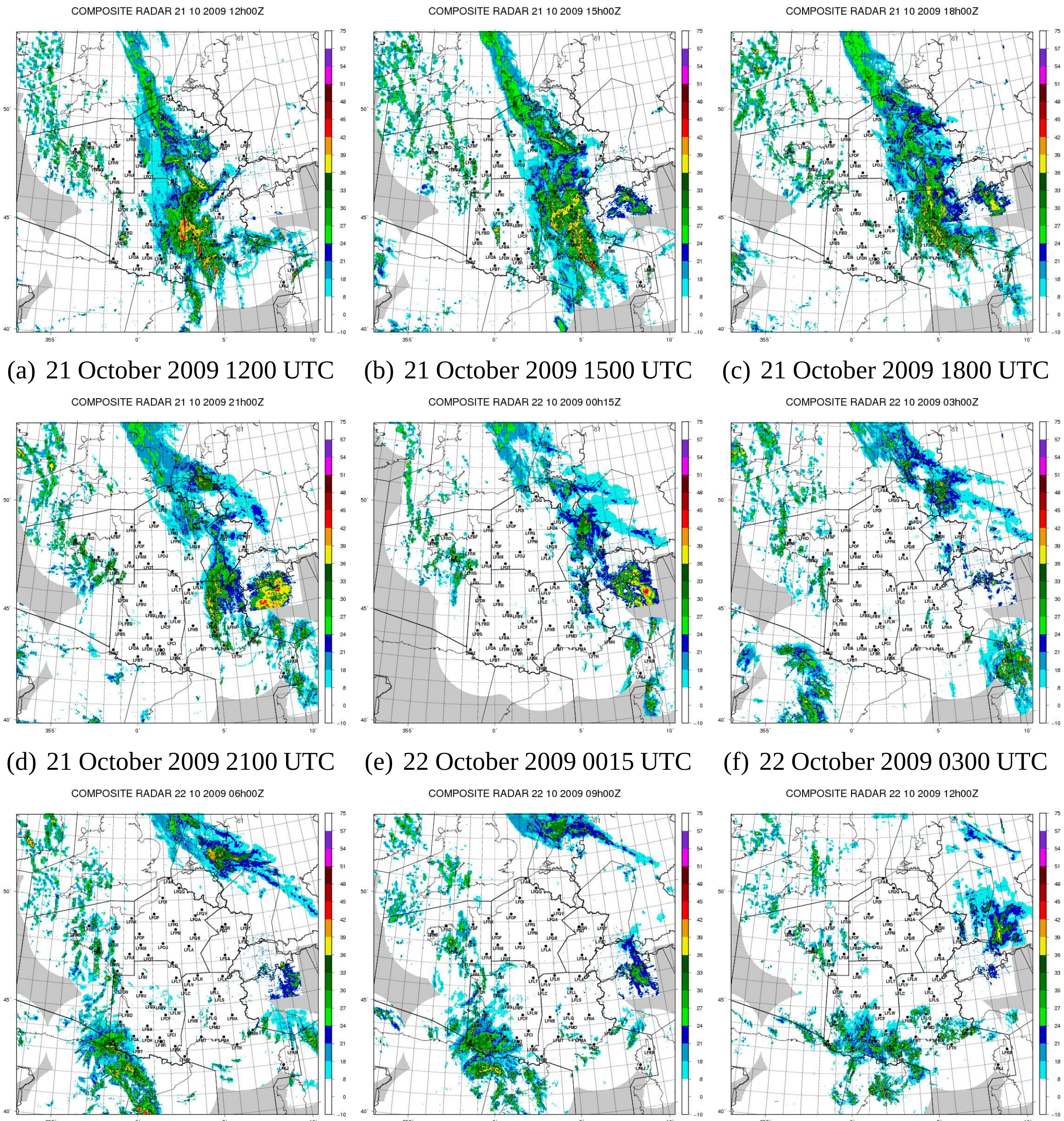

(a) 21 October 2009 1200 UTC (b) 21 October 2009 1500 UTC (c) 21 October 2009 1800 UTC

(d) 21 October 2009 2100 UTC (e) 22 October 2009 0015 UTC (f) 22 October 2009 0300 UTC

(g) 22 October 2009 0600 UTC (h) 22 October 2009 0900 UTC (i) 22 October 2009 1200 UTC

Figure B.1: Reflectivity composite [dBZ].

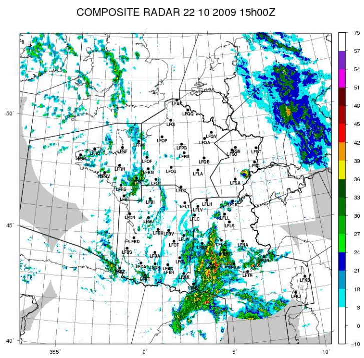

(a) 22 October 2009 1500 UTC

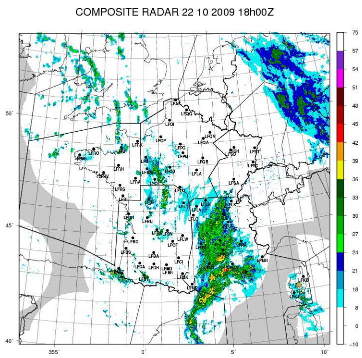

(b) 22 October 2009 1800 UTC

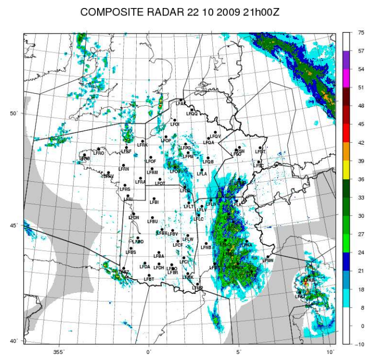

(c) 22 October 2009 2100 UTC

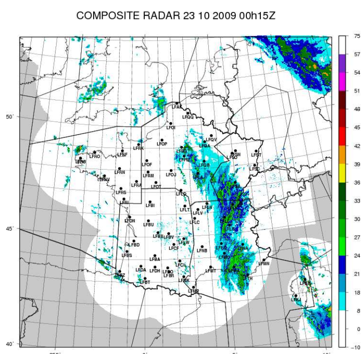

(d) 23 October 2009 0015 UTC

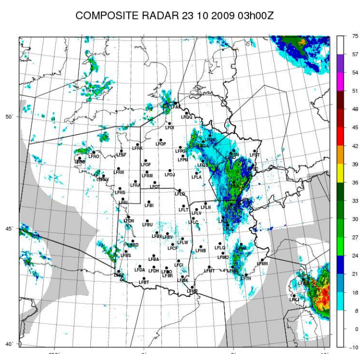

(e) 23 October 2009 0300 UTC

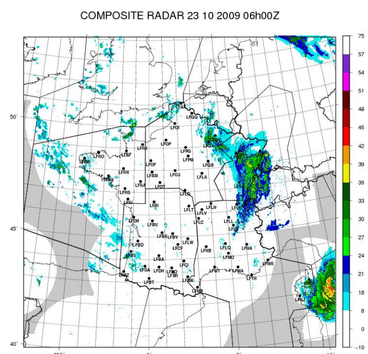

(f) 23 October 2009 0600 UTC

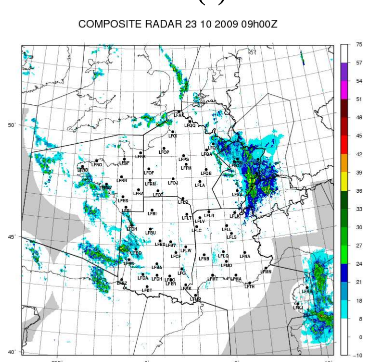

(g) 23 October 2009 0900 UTC

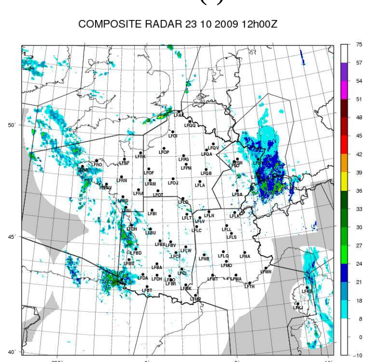

(h) 23 October 2009 1200 UTC

Figure B.2: Reflectivity composite [dBZ].

C Modifications in the source code

All modifications are marked with “ghb” and “ghe”.

1. `odb/pandor/module/bator_decodbufr_mod.F90`
2. `odb/pandor/module/bator_ecritures_mod.F90`
3. `arp/op_obs/reflsim_2dop.F90`
4. `odb/ddl/satbody_radar.sql`
5. `bla/mf_blacklist.b`
6. `odb/ddl.ECMA`
   `ln -s ../ddl/satbody_radar.sql satbody_radar.sql`

References

Bech, J., U. Gjertsen, and G. Haase, 2007: Modelling weather radar beam propagation and topographical blockage at northern high latitudes. *Q. J. R. Meteorol. Soc.*, **133**, 1191–1204.

Caumont, O., V. Ducrocq, G. Delrieu, M. Gosset, J.-P. Pinty, J. P. du Châtelet, H. Andrieu, Y. Lemaître, and G. Scialom, 2006: A radar simulator for high-resolution nonhydrostatic models. *J. Atmos. Oceanic Technol.*, **23**, 1049–1067.

Delrieu, G., J.-D. Creutin, and H. Andrieu, 1995: Simulation of radar mountain returns using a digitized terrain model. *J. Atmos. Oceanic Technol.*, **12**, 1038–1049.

Germann, U. and J. Joss, 2003: Operational measurement of precipitation in mountainous terrain. In *Weather Radar - Principles and Advanced Applications*, Meischner, P., editor. Springer Verlag, 52–77. 337 pp.

Gjertsen, U. and J. I. Dahl, 2002: Challenges for precipitation estimation in mountainous regions. In *Proc. ERAD (2002)*, EMS, Copernicus GmbH, 250-254.

Montmerle, T., E. Wattrelot, C. Faccani, O. Caumont, M. Jurasek, and G. Haase, 2008: Regional scale assimilation of radar data at mto-france. In *SRNWP Workshop on Data Assimilation, 21-23 March 2007, Norrköping (Sweden)*.

Parent du Châtelet, J., P. Tabary, C. Gueguen, and B. Fradon, 2006: The meteo-france single-radar and composite qpe operational products. In *Proc. ERAD (2006)*, 299-302.

Wattrelot, E., O. Caumont, S. Pradier-Vabre, M. Jurasek, and G. Haase, 2008: 1D+3DVar assimilation of radar reflectivities in the pre-operational AROME model at Météo-France. In *Proc. ERAD (2008)*.